The value of dynamic MRI studies in parotid tumors

Sedat Alibek, Johannes Zenk, Alessandro Bozzato, Michael Lell, Markus Grunewald, Katharina Anders, Christina Rabe, Heinrich Iro, Werner Bautz, Holger Greess

The Value of Dynamic MRI Studies in Parotid Tumors[1]

Sedat Alibek, MD, Johannes Zenk, MD, Alessandro Bozzato, MD, Michael Lell, MD, Markus Grunewald, MD
Katharina Anders, MD, Christina Rabe, Heinrich Iro, MD, Werner Bautz, MD, Holger Greess, MD

Salivary gland neoplasms account for about 0.5%–3% of all malignant tumors (1–4), and most individuals suffer from some illness related to the salivary glands once in their lifetime—infectious as well as neoplastic or part of a

systemic disease, acute or chronic (1). Determining whether a parotid mass is benign or malignant is very important because it strongly influences therapy: if a tumor is benign, only partial or even extracapsular dissection might be indicated, whereas total or even radical parotidectomy including facial nerve resection is necessary whenever a malignant lesion is suspected.

The diagnostic strategy is a multimodal approach. The most inexpensive and well-established diagnostic tool after physical examination is ultrasound (5). High sensitivities up to 100% are reported in literature for tumors arising in the superficial lobe of the parotid gland (4). Ultrasound proved to be very suitable to differentiate between intra- versus extraglandular lesions. For tumors

located in deeper parts of the gland, cross-sectional imaging such as computed tomography (CT) and magnetic resonance imaging (MRI) are necessary (6). Since the 1980s, CT has become increasingly useful for demonstrating tumors of the salivary glands and their extent as well as differentiating tumors of the salivary glands from extrinsic lesions (7–10). The limitations of CT, such as radiation and use of iodinated contrast agents with relatively high rate of side effects, encourage the use of MRI as the standard imaging modality for salivary gland tumors. The possibility of direct multiplanar imaging, excellent tissue contrast with better evaluation of the interfaces between muscle and tumor (which exhibit very similar density values in CT), and better differentiation of intrinsic versus extrinsic masses have made MRI the imaging modality of choice (11,12). It has been shown that MRI studies are superior in detecting and determining the extent of disease in the setting of suspected salivary gland mass (1). Most of these studies were done with 0.5 T magnets. The use of 1.5 T magnets improves image quality, because shorter acquisition times allow dynamic MRI studies that add precious information regarding tumor vascularization, perfusion, contrast uptake, and washout (13). Yet it can be difficult to determine the tumor entity with conventional MRI studies.

Because true multimodality approaches for salivary gland tumors are not feasible for economic considerations (14), imaging modalities covering the needs of clinicians, radiologists, surgeons, and oncologists all at once would be the ideal solution in the diagnostic-therapeutic algorithm.

To add a powerful tool to MRI scans, in this study we evaluated the value of dynamic MRI studies in patients with clinically suspected parotid masses. The purpose of this study is also to examine tumor signal characteristics in dynamic contrast-enhanced MRI to better differentiate between benign and malignant lesions and improve presurgical therapy planning.

MATERIALS AND METHODS

Between July 2002 and January 2004, 112 consecutive patients (55 male, 57 female, ages 11–86 years, mean age 54 years) presenting with a palpable parotid mass were examined with dynamic contrast-enhanced MRI on a 1.5-T MR scanner (Magnetom Symphony, Siemens, Erlangen/Germany) in a prospective study. Approval of the local ethical committee and written

informed consent for each patient was obtained. The MRI study protocol consisted of localizer sequences in transversal, sagittal, and coronal planes followed by a T2-weighted rephased Short-Tau Inversion Recovery (STIR) sequence in the coronal plane and a transversal T2-weighted STIR and T1-weighted rephased Spin-Echo (SE) sequence (repetition time/echo time: 3,440/105 and 525/17, respectively; matrix: 256 × 256; number of slices: 19; slice thickness: 4 mm; gap: 10%; field of view 220 mm). After detecting the mass in T1-weighted and T2-weighted images, we selected corresponding slice positions for a T1-weighted FLASH sequence (repetition time: 60, echo time: 5.6) in the transversal plane, used for the dynamic contrast study. A stack of five slices was positioned to ensure coverage of the center of the parotid tumor. Each patient received intravenous contrast injection (weight-adapted dosage, 0.2 mL gadolinium per kilogram body weight) with a flow rate of 1.0 mL/second. The contrast agent application and the T1-weighted FLASH sequence were started simultaneously. Ten acquisitions of 10 seconds each were performed resulting in a total scan time of 1:40 minutes for the dynamic study. The examination was then completed by T1-weighted postcontrast rephased SE FATSAT sequences (repetition time: 466, echo time: 17) in the transversal and coronal plane (matrix: 256 × 256; number of slices: 19; slice thickness: 4/6 mm; gap: 10%; field of view 220/230–260 mm, respectively). Signal intensity versus time curves were obtained in regions of interest (ROI) from the dynamic FLASH sequence (Fig 1), using a dedicated software tool (Mean Curve, Siemens Medical). The slice displaying the largest lesion diameter was used for positioning of the ROI. For tumors with a heterogeneous morphology, we used one ROI for each area and obtained several signal versus time curves (Fig 2).

First, the conventional MRIs were read by three experienced radiologists and a diagnosis was established in consensus. At the time of the reading session, the patients did not have surgery or biopsy for histopathologic workup of the parotid tumor yet. All patients underwent surgery with histopathologic workup. The MRI diagnosis was then compared with the histopathology reports. Then signal intensity versus time (SIvT) curves were obtained for all parotid gland tumors, which were then evaluated, categorized and compared according to the histopathological results. Finally all MRI datasets were re-read together with the tumour specific SIvT curves and correlated again with the histopathological diagnosis.
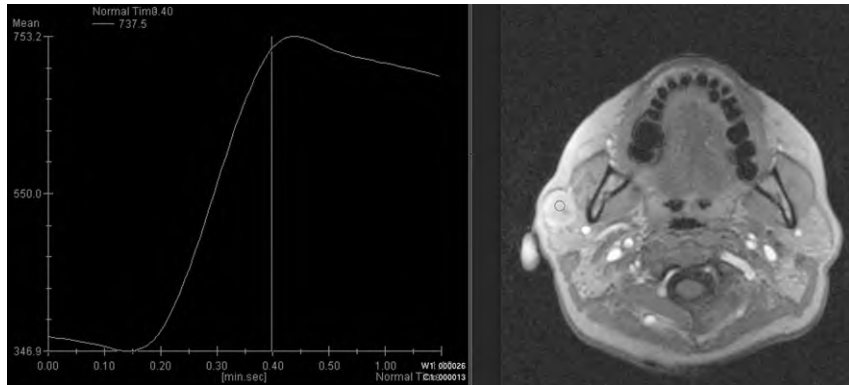
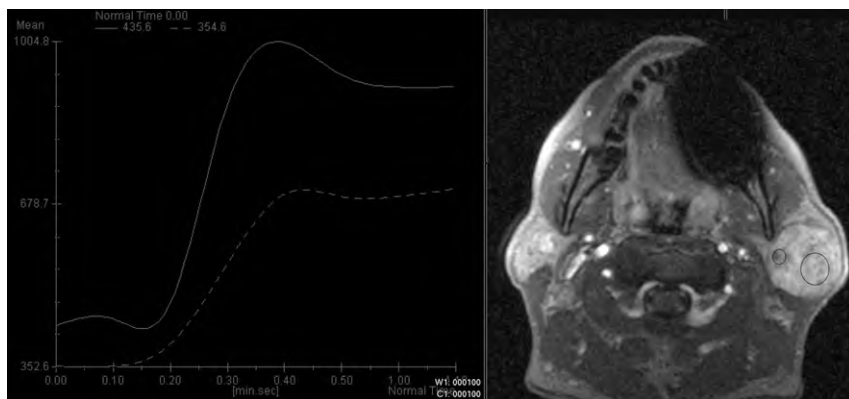**Figure 1.** Single region of interest in tumor with homogenous morphology.

Figure 2. Two regions of interest in tumor with inhomogeneous morphology.

RESULTS

The histopathology work-up of the specimens obtained at surgery revealed Pleomorphic adenoma (n = 46), adenolymphoma (Warthin-Tumors) (n = 24), other benign entities (n = 29), and carcinoma (n = 13) (Table 1). All carcinomas were high grade carcinomas, low grade malignancies such as lymphoma were not found.

Typical signal characteristics were seen in cross sectional pre- and postcontrast images. Pleomorphic adenomas as well as malignant tumors showed hyperintense signal on T2-weighted images, adenolymphomas showed hypointense to intermediate signal on T2-weighted images. Pleomorphic adenomas as well as malignant tumors were hypointense on T1-weighted images, whereas adenolymphomas showed a slightly hyperintense signal, probably due to proteinaceous tumour portions. After administration of contrast medium, pleomorphic adenomas enhanced mildly whereas adenolymphoma and malignant tumors showed a strong enhancement.

Table 1
Tumor Entities and Distribution

Tumor Entity	n	Proportion
Pleomorphic adenoma	46	41.1%
Adenolymphoma	24	21.4%
Carcinoma	13	11.6%
Lymph nodes	7	6.3%
Oncocytoma	4	3.6%
Hemangioma	3	2.7%
Lymphangioma	3	2.7%
Cysts	3	2.7%
Sarcoidosis	2	1.8%
Basal cell adenoma	2	1.8%
Papillary cystadenoma	2	1.8%
Angiomyoma	2	1.8%
Scar tissue	1	0.9%

Four typical SIvT curves could be seen for the most common benign and malignant parotid tumors.

After contrast injection, pleomorphic adenomas showed a slow and gradual increase of signal intensity followed by a plateau phase on a low intensity level, whereas the
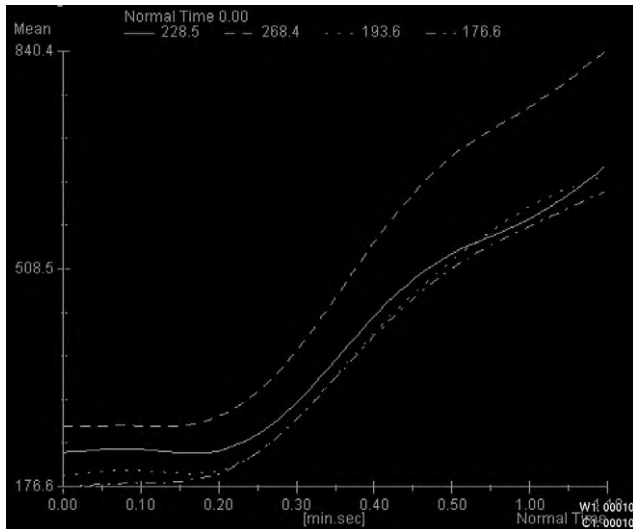
Figure 3. Typical signal intensity versus time curves of a pleomorphic adenoma in different regions of interest.
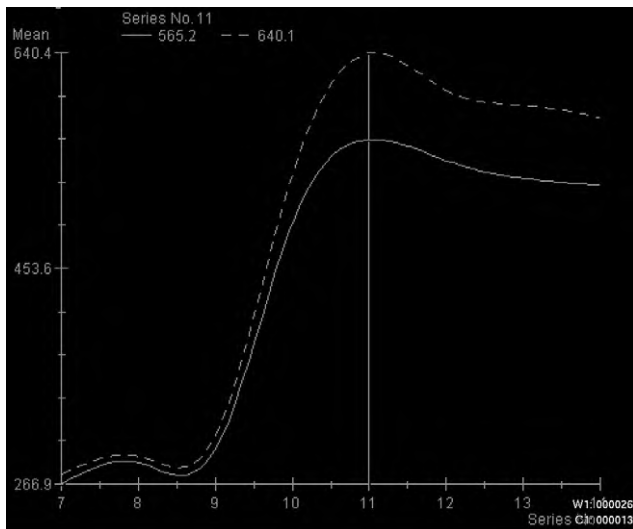

Figure 4. Typical signal intensity versus time curves of an adenolymphoma in different regions of interest.

SIvT curve of adenolymphomas showed a rapid increase of the SI level followed by a plateau phase at a high signal intensity level (Fig 3, 4). The Wilcoxon-Mann-Whitney U-test revealed statistic significance ($P = .0011$ and $P < .001$) between the time-to-peak curves of pleomorphic adenomas and adenolymphomas, each compared with all other lesions (Table 2). No significant difference was found for total peak SI values ($P = .1033$ and $P = .3432$ respectively) (Table 3). Receiver operating characteristic (ROC) analysis was used to evaluate the ability of the variables to discriminate between tumors. The optimal

cutpoint was selected as the maximum sum of sensitivity and specificity (Youden's index) and was >50 seconds for pleomorphic adenomas and <102 seconds for adenolymphomas (Tables 4 and 5).

The characteristic finding of cysts in dynamic MRI was a lack of signal increase after administration of intravenous contrast material; the vacillate course of the SIvT curve at a low signal level is explained with imaging artefacts (Fig 5).

Although malignant parotid tumors have a great variety of histologic origin, the typical SIvT curve showed a rapid increase of signal intensity with a high peak level and was followed by a plateau phase at high signal intensities. The SIvT curve of malignant tumors was similar to that of adenolymphomas (Fig 6). Benign lesions showed peak signal intensities between 84 and 1,194; malignant lesions showed peak intensities between 333 and 987. The Wilcoxon-Mann-Whitney U-test showed a statistically significant difference between the distributions of peak SI values comparing malignant tumors with benign tumors ($P = .0049$) and malignant tumors with pleomorphic adenomas ($P = .0033$), but no statistical significance when comparing malignant tumors with adenolymphoma ($P = .0724$).

No significant difference was found for time to peak values comparing malignant tumors with benign tumors ($P = .4098$) or malignant tumors with pleomorphic adenomas ($P = .9654$), and no significance but a trend when comparing malignant tumors with adenolymphoma ($P = .0833$) (Table 6). ROC analysis was used to evaluate the ability of the variables to discriminate between tumors. The optimal cut point was selected as the maximum sum of sensitivity and specificity (Youden's index) and was >710.50 for malignant tumors (Tables 7 and 8). In contrast to this, adenolymphomas showed lower peak levels between 151 and 914 (Table 3). So the maximum peak value can be a valuable criterion to differentiate between malignant tumors and benign entities, pleomorphic adenoma, respectively.

When reading only the conventional cross sectional pre- and post-contrast MRIs, 92% of tumors (103 of 112) could be classified correctly (benign versus malignant); 8% (9 of 112) were misclassified. Malignant tumors were assigned correctly in only 38.5% (5/13) (Table 9).

Pleomorphic adenomas were correctly diagnosed in 89.1% (41/46) and adenolymphomas only in 25% (6/24). Adenolymphomas were misdiagnosed in 54.2% as pleomorphic adenomas (13/24), whereas only 6.5% pleomor-

Table 2
Distribution of Time to Peak (TTP) Values Among Pleomorphic Adenomas

Variable	Tumor	n	Median	Mean	SD	Min	Q1	Q3	Max	P Value
TTPs	Others	58	49.00	80.59	57.05	18.00	41.00	110.00	335.00	
	Pleomorphic adenoma	43	110.00	99.93	30.00	43.00	100.00	110.00	205.00	.0011
TTPs	Others	79	110.00	97.28	49.26	18.00	49.00	110.00	335.00	
	Adenolymphoma	22	47.00	58.45	28.75	32.00	41.00	67.00	151.00	<.001

Adenomas, adenolymphomas, and other entities and corresponding P values obtained from the Wilcoxon-Mann-Whitney U-test.

Table 3
Distribution of Peak Signal Intensities (SI) Values Among Pleomorphic Adenomas

Variable	Tumor	n	Median	Mean	SD	Min	Q1	Q3	Max	P Value
Peak (SI)	Others	57	480.00	511.42	241.25	84.20	342.20	692.40	1194.8	
	Pleomorphic adenomas	43	421.90	434.98	174.38	173.70	276.80	551.20	899.00	.1033
Peak (SI)	Others	79	435.20	472.17	227.31	84.20	308.70	600.20	1194.8	
	Adeno-lymphoma	21	508.60	502.57	178.04	151.50	410.50	551.00	914.10	.3432

Adenomas, adenolymphomas, and other entities and corresponding P values obtained from the Wilcoxon-Mann-Whitney U-test.

Table 4
Optimal Cut Points from Receiver Operating Characteristic Analysis for Time to Peak (TTP)

Variable	Cutpoint	Sensitivity	Specificity	Youden
TTPs for pleomorphic adenomas	>50.00	0.884	0.517	0.401
TTPs for adenolymphoma	<102.00	0.909	0.646	0.555

phic adenomas were misdiagnosed as adenolymphomas (3/46) (Table 10).

Reading the conventional images together with the SIvT curves of the dynamic study led to a correct diagnosis in 92% of adenolymphomas (22/24), 100% of pleomorphic adenomas (46/46), and 85% (11/13) of malignant tumors of the parotid gland.

Our dynamic MR study required 1:40 minutes of additional scan time per patient. Loading the dynamic cross sectional images into our dedicated software (Mean Curve, Siemens Medical Solutions, Erlangen/Germany), defining the ROIs and calculating the SIvT curves added less then 2 minutes of postprocessing time. The evaluation of the graphs took about 30 seconds per patient. So the additional examination time was less then 2 minutes per patient with an additional evaluation and reading time for the radiologist of less then 2.5 minutes.

DISCUSSION

To reliably differentiate benign from malignant parotid masses is of fundamental concern, because it strongly influences therapeutic decisions: extracapsular dissection, partial parotidectomy versus radical parotidectomy with removal of the facial nerve are possible surgical strategies. Although biopsy is still a gold standard in diagnosis of parotid tumors (1,4,12,15), given the technical developments of the last 20 years imaging modalities such as ultrasonography, CT, and MRI, can provide important diagnostic information and prevent unnecessary biopsy in clinically suspected tumors of the parotid gland (15,16). Ultrasound is a low-cost, widely available but user-dependant modality that has a high sensitivity for detection of parotid tumors located in the superficial lobe but might be less significant in detecting tumors of the deeper lobe. Cross-sectional imaging modalities are helpful for correct presurgical planning (18). CT is a widely available and fast imaging modality, which provides excellent information about tumour localization and expansion, but is combined with x-ray exposure and side effects of contrast media use (14). MRI offers superior soft tissue contrast and does not use x-ray; side effects of contrast media administration are scarcely to be expected. Although some authors claim that—with respect to the presurgical planning and contribution to the diagnosis and therapy planning of parotid tumors—CT and MRI provide the same

Table 5
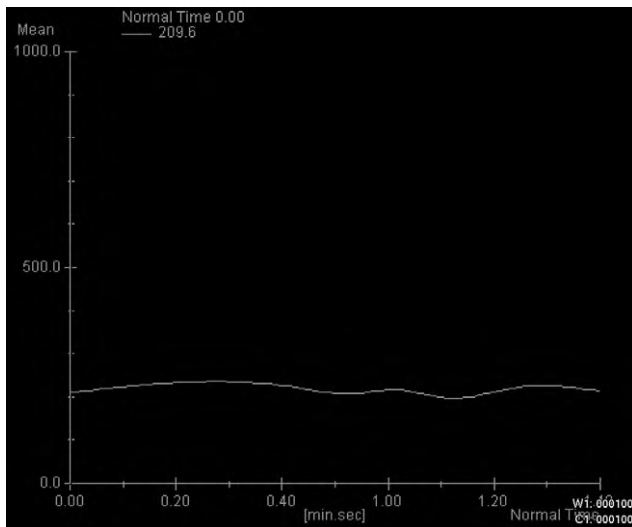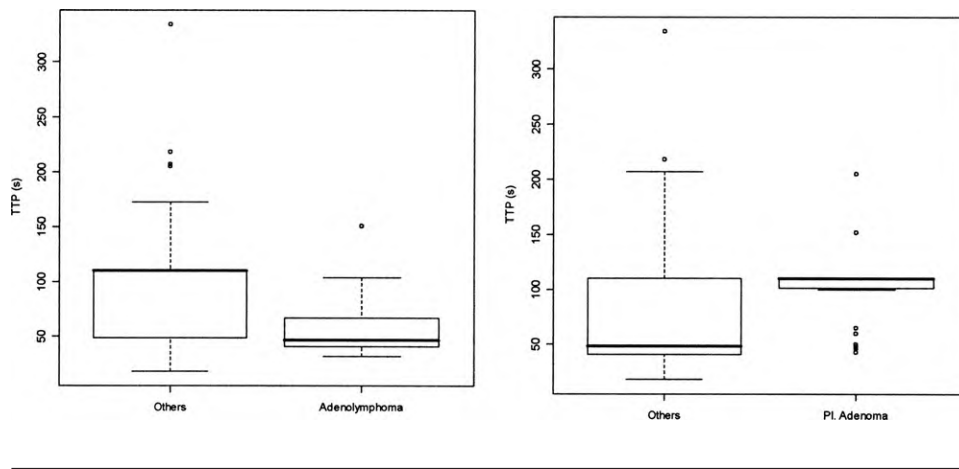**Box Plots for Time to Peak Value of Pleomorphic Adenomas and Adenolymphomas**

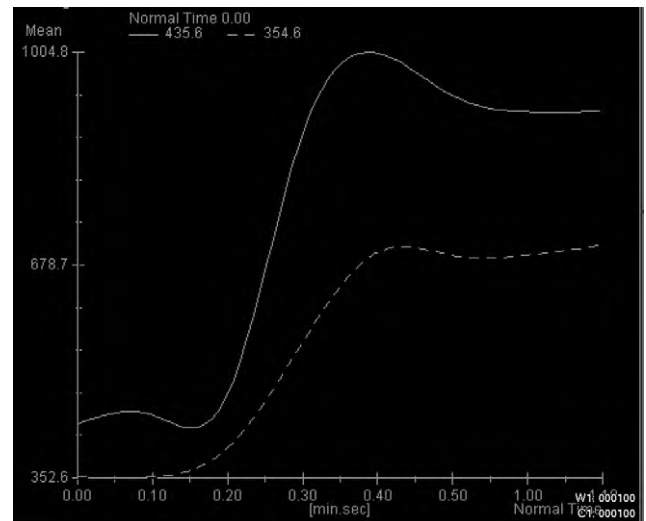Figure 5. Typical signal intensity versus time curve of a cyst.

Figure 6. Typical signal intensity versus time curve of a malignant tumor in different regions of interest.

information (14,19), others state that CT is less accurate than MRI concerning extent of disease (20). In our opinion, MRI is the modality of choice, because MRI enables excellent delineation of soft-tissue masses and infiltration of neighboring structures (21). Furthermore, with dynamic MRI and the use of SIvT curves, we may more reliably predict whether a parotid tumor is benign or malignant (22).

The typical features of pleomorphic adenomas in conventional and dynamic MRI are a well-circumscript, smooth surface, although histologically it does not exhibit a true capsule but a pseudocapsule with small pseudopodia (23,24). Sometimes the surface is lobulated. The tumor usually appears as a solitary lesion, but reportedly

recurrent pleomorphic adenoma can appear with multiple lesions (24). The tumor shows low signal intensity on T1-weighted precontrast images, high signal intensity on T2-weighted images, and enhances mildly after contrast media administration. As the name indicates, the tumor has a great histologic diversity, which can be seen in the inhomogeneous signal intensity on T2-weighted images. The epithelial tissue is intermingled with myxoid, mucoid, or chondroid areas displaying more or less high signal intensity on T2-weighted images (25,26). In our series, less then 10% of the pleomorphic adenomas showed inhomogeneous signal intensity on T2-weighted images. More than 90% showed high signal intensity on T2-weighted

Table 6
*P Value of the Wilcoxon-Mann-Whitney Test for Comparison with Malignant Tumors, Respectively

Variable	Tumor	n	Median	Mean	SD	Min	Q1	Q3	Max	P Value*
Peak (signal	All benign	88	446.00	453.86	205.50	84.20	304.35	557.60	1194.80	.0049
intensity)	Adenolymphoma	21	508.60	502.57	178.04	151.50	410.50	551.00	914.10	.0724
	Pleomorphic adenomas	43	421.90	434.98	174.38	173.70	276.80	551.20	899.00	.0033
	Malignant	12	643.00	659.64	225.32	333.50	455.10	880.65	987.70	
Time to peak (s)	All benign	89	103.00	84.92	38.60	18.00	47.00	110.00	207.00	.4098
	Adenolymphoma	22	47.00	58.45	28.75	32.00	41.00	67.00	151.00	.0833
	Pleomorphic adenomas	43	110.00	99.93	30.00	43.00	100.00	110.00	205.00	.9654
	Malignant	12	106.50	117.75	90.49	35.00	43.00	153.50	335.00	

Table 7
Optimal Cut Points from the Receiver Operating Characteristic Analysis for Peak Signal Intensity of Malignant Tumors

Variable	Cutpoint	Sensitivity	Specificity	Youden
Peak (signal intensity)	710.50	0.500	0.909	0.409

Table 8
Box Plots for Peak Signal Intensity Values of Malignant and Benign Tumors

Table 9
Classification of Benign/Malignant Tumors by Conventional Magnetic Resonance Imaging

Conventional Magnetic Resonance Imaging Diagnosis	Histopathologic Finding		n
	Benign	Malignant	
Benign	98	8	106
Malignant	1	5	6
n	99	13	112
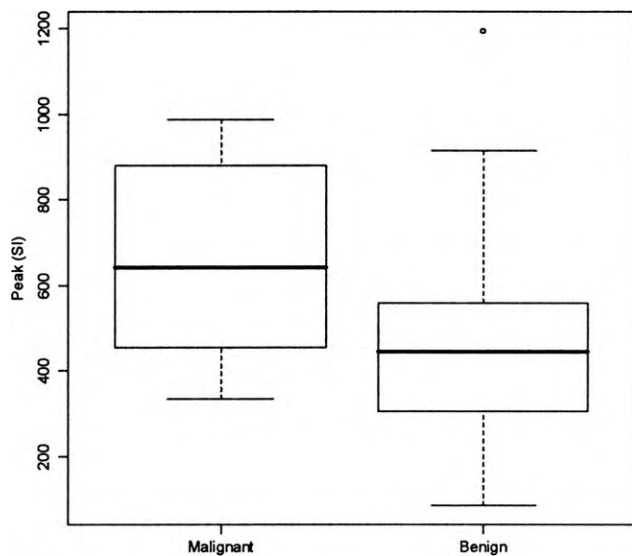
images (Table 11). In dynamic MRI, all pleomorphic adenomas showed a characteristic gradual increase of the SIvT curve followed by a plateau phase on a low intensity level (Fig 4). Statistical significance was achieved in the Wilcoxon test for the time to peak value of pleomorphic adenomas (Table 2). Neither the largest diameter of the tumor nor the (in)homogeneity of the tumor led to changes of the typical SIvT curve when defining the solid portions as ROIs.

Adenolymphomas (Warthin's tumor) are encapsulated and have a round or oval shape with a smooth or lobulated surface. Adenolymphomas are often located bilaterally and seen in older patients. Cystic parts are seen in up to 30% (23) and contain proteinaceous or viscous fluid, causing a shortening of T1 relaxation time. Solid portions consisting of epithelial tissue and lymphoid proliferation usually show no enhancement after contrast media administration. The tumor shows intermediate signal intensity on T2-weighted images, mixed signal intensity on T1-weighted images with high signal in the cystic (proteinaceous) parts and low signal in the solid parts, and intermediate to high signal intensity after contrast media administration (16,27). In our series, we saw mixed signal intensities on T2-weighted images, and about 30% of the tumors showed increased signal intensity on T1-weighted images before contrast media administration. About 90% showed high signal intensity after contrast media administration (Table 11). Statistical significance was seen for the time to peak values with steep rise of the SIvT curves (Table 2), followed by a plateau phase at a high signal intensity level (Fig 4). This enabled us to differentiate

Table 10
Correct/False Classifications on Conventional Magnetic Resonance Imaging

Magnetic Resonance Imaging Diagnosis	Histopathology Finding			
	Adenolymphoma	Pleomorphic Adenoma	Others	n
Adenolymphoma	6	3	6	15
Pleomorphic adenoma	13	41	16	70
Others	5	2	20	27
n	24	46	42	112

Table 11
Tumor Signal Characteristics on T2-Weighted/T1-Weighted/T1-Weighted + GD Images

Tumor Entity	T2-weighted	T1-weighted	T1-weighted + GD
Adenolymphoma	Low/intermediate	Low/intermediate	High
Pleomorphic adenoma	High	Low	Intermediate
Carcinoma	High	Low	High

between benign entities (eg, pleomorphic adenoma versus adenolymphoma), which is not always possible on conventional MRI scans.

Cysts histologically represent lymphoepithelial cyst or retention cyst (16); round shape, homogenous high signal intensity on T2-weighted images, well-defined borders, and a smooth contour together with low signal intensity on T1-weighted images before and after contrast administration are typical characteristics of cysts. The characteristic feature at dynamic MRI is a vacillating SIvT curve at a low signal intensity level (Fig 5).

Malignant parotid tumors (eg, carcinomas) represent predominantly squamous cell carcinoma, undifferentiated carcinoma, adenocarcinoma, mucoepidermoid carcinoma, adenoid cystic carcinoma, or acinic cell carcinoma (23). It is not possible to determine a specific histologic diagnosis with MRI, but differentiation between benign and malignant tumors is possible. Highly malignant tumors usually display irregular tumor margins and show infiltration into adjacent structures. Because of different tumor entities and necrotic or solid areas within the tumor, a mixed signal intensity is seen on MRI. T2-weighted images appear with heterogenous signal intensity, low within the solid portions and high in necrotic parts, T1-weighted images are mostly of low signal intensity and a heterogenous contrast media uptake is represented by heterogenous high signal intensity on postcontrast T1-weighted images. We can find similar results in our series of malignant parotid tumors (Table 11). The SIvT curves show similar characteristics as seen in adenolymphomas with a rapid increase

in signal intensity followed by a plateau phase at a high signal level (Fig 6). Statistical significance was found for the peak signal intensity values of carcinomas compared with the group of all benign entities and compared with the group of pleomorphic adenomas (Table 6). No statistical significance was found when comparing peak signal intensities when comparing malignancies with the group of adenolymphomas, but only a statistic trend, possibly a result of the low number of malignancies (n = 13) in our study group.

Differentiation of benign and malignant parotid tumors is difficult because of the histologic variety of tumors; thus, different diagnostic approaches to parotid tumour imaging have been investigated and published in the last 10 years. T2-weighted MRI has been shown to be a reliable predictor (73%) of whether a tumor is benign or malignant (27,28). The basic rule is that a hyperintense mass in T2-weighted images is benign, whereas a mass with low to intermediate signal intensity on T2-weighted images is likely to be malignant. Other authors have implied that signal intensity in T2-weighted images is not helpful (30,31). In our series, we found that about 80% of malignant parotid tumors, 75% of pleomorphic adenomas, and only 30% of adenolymphomas showed high signal intensity in T2-weighted imaging (Table 11). Differentiation of head and neck lesions with diffusion-weighted MRI may provide supplementary information before surgery and biopsy (32). Another interesting aspect was shown by Sakamoto et al with heavily T2-weighted MRI. They could show that neither homogeneity nor signal intensity

differed significantly in conventional T2-weighted images among adenolymphomas, pleomorphic adenoma, and malignant tumors in conventional T2-weighted imaging, but signal intensity in these three tumor types were significantly different in solid portions when using heavily T2-weighted imaging (33).

The use of dynamic contrast-enhanced MRI represents a different approach. Yabuuchi et al could show that the most common tumor types in the parotid gland show specific contrast enhancement characteristics and—together with delayed phase scanning and so-called washout ratios—a better differentiation is possible (13). These studies were done retrospectively and with a low number of patients (n = 29) with 0.5 T scanner. Our study is a prospective MRI study of parotid tumors using a 1.5 T scanner, with a considerable number of patients.

The additional data acquisition time for dynamic imaging is less than 2 minutes, and postprocessing (selecting the relevant slice positions, drawing ROIs, and calculating the SIvT curve) can be completed in about 2.5 minutes. So an additional time need of less than 5 minutes (total time for conventional imaging sequences: approximately 20–25 minutes) is counterbalanced by accuracy rates of about 85% for detecting malignant lesions. With 1.5-T MRI scanners, we get better SIvT curves because of the shorter imaging time per acquisition. In our series, we could considerably improve our diagnoses with the additional dynamic series (SIvT curves) and no further needs for delayed imaging and other parameters (eg, washout ratios) arose.

According to the results of this investigative study, we will use dynamic MRI imaging of tumors of the head and neck region in our clinical routine. With this method, we are not only able to better differentiate malignant versus benign lesions, but also detect occult malignant lesions without a facial nerve palsy, which is very often the first clinical sign for the existence of a malignancy of the parotid gland.

CONCLUSION

Dynamic contrast-enhanced MRI at 1.5T field strength allows a better differentiation between the common parotid tumors (pleomorphic adenoma, adenolymphoma, high-grade malignancies [ie, carcinomas]) before surgery without need for invasive diagnostic tools (eg, biopsy). The additional time needed for dynamic imaging sequences is less than 2 minutes and, with dedicated soft-

ware, quick and accurate evaluation of the signal characteristics of tumor entities is possible. Time-to-peak curves and maximum SI values show statistical significance and prove to be very helpful in deciding whether a parotid tumour is benign or malignant, even in clinically occult malignant lesions.

However, further morphologic features such as sharp or blurred borders, invasion of neighboring structures, and clinical signs of malignancy are still important to establish the correct diagnosis (17,29).

REFERENCES

1. Yousem DM, Kraut MA, Chalian AA. Major salivary gland imaging. Radiology 2000; 216:19–29.
2. Donath K, Ussmuller J. Aetiopathogenese und histopathologie der speicheldruesenerkrankungen. Laryngo-Rhino-Otol 2001; 80(Suppl 1):1–25.
3. Greess H, Lell M, Römer W, et al. Indikation und aussagekraft von CT und MRT im Kopf-Hals-Bereich. HNO 2002; 50:611–625.
4. Licitra L, Grande C, Prott FJ, et al. Major and minor salivary gland tumors. Crit Rev Oncol Hematol 2003; 45:215–225.
5. Zenk J, Iro H. Doppler-und farbkodierte duplexsonographie im Kopf-Hals-Bereich. In: Kopf-Hals-Sonographie. Berlin: Springer Verlag, 2000; 75–96.
6. Gritzmann N, Rettenbacher T, Hollerweger A, et al. Sonography of the salivary glands. Eur Radiol 2003; 13:964–975.
7. Casselman JW, Mancuso AA. Major salivary glands masses; comparison of MR imaging and CT. Radiology 1987; 165:183–189.
8. Mancuso AA, Hanefee WN. Salivary glands. In: Computed tomography and magnetic resonance imaging of the head and neck, 2nd ed. Baltimore: Williams and Wilkins, 1985; 139–160.
9. Som PM, Saunders DE. The salivary glands. In: Bergeron RT, Osborn AG, Som PM, Head and neck imaging excluding the brain. St Louis, Mo: Mosby, 1986; 186–234.
10. Lev MH, Khanduja K, Morris PP, et al. Parotid pleomorphic adenomas: delayed CT enhancement. AJNR Am J Neuroradiol 1998; 19:1935–1939.
11. Szolar DH, Groell R, Braun H. Ultrafast computed tomography and three-dimensional image processing of CT sialography in patients with parotid masses poorly defined by magnetic resonance imaging. Acta Otolaryngol (Stockh) 1996; 116:112–118.
12. Paris J, Facon F, Pascal T, et al. Preoperative diagnostic values of fine-needle cytology and MRI in parotid gland tumors. Eur Arch Otorhinolaryngol 2005; 262:27–31.
13. Yabuuchi H, Fukuya T, Tajima T, et al. Salivary gland tumors: diagnostic value of gadolinium-enhanced dynamic MR imaging with histopathologic correlation. Radiology 2003; 226:345–354.
14. Koyuncu M, Sesen T, Akan H et al. Comparison of computed tomography and magnetic resonance imaging in the diagnosis of parotid tumors. Otolaryngol Head Neck 2003; 129:726–732.
15. Fischer T, Filimonow S, Petersein J, et al. Diagnosis of Heerfordt's syndrome by state-of-the-art ultrasound in combination with parotid biopsy: a case report. Eur Radiol 2002; 12:134–137.
16. Kinoshita T, Ishii K, Naganuma H. MR imaging findings of parotid tumors with pathologic diagnostic clues. A pictorial essay. J Clin Imaging 2004; 28:93–101.
17. Vogl TJ, Dresel SH, Grevers G, et al. Sjoegren's syndrome: MR imaging of the parotid gland. Eur Radiol 1996; 6:46–51.
18. Shah GV. MR imaging of salivary glands. Neuroimaging Clin N Am 2004; 14:777–808.
19. Som PM, Sacher M, Stollman AL. Common tumors of the parapharyngeal space: refined imaging diagnosis. Radiology 1998; 169:81–85.
20. Kaneda T, Minami M, Ozawa K. Imaging tumors of the minor salivary glands. Oral Radiol Endocrinol 2003; 78:385–390.
21. Okahara M, Kiyosue H, Hori Y, et al. Parotid tumors: MR imaging with pathological correlation. Eur Radiol 2003; 13(Suppl 4):25–33.

22. Shah GV, Fischbein NJ, Patel R, et al. Newer MR imaging techniques for head and neck. Magn Reson Imaging Clin N Am 1979; 11:449–469.

23. Batsakis JG. Tumors of the major salivary glands. In: Batsakis JG, Tumors of the head and neck, clinical and pathological considerations. Baltimore, Md: Williams & Wilkins, 1979; 1–75.

24. Koral K, Sayre J, Bhuta S, et al. Recurrent pleomorphic adenoma of the parotid gland in pediatric and adult patients: value of multiple lesions as a diagnostic indicator. AJR Am J Roentgenol 2003; 180:1171–1174.

25. Ikeda K, Katoh T, Ha-Kawa SK, et al. The usefulness of MR in establishing the diagnosis of parotid pleomorphic adenoma. Am J Neuroradiol 1996; 17:555–559.

26. Tsushima Y, Matsumoto M, Endo K, et al. Characteristic bright signal of parotid pleomorphic adenomas on T2-weighted MR images with pathological correlation. Clin Radiol 1994; 49:485–489.

27. Hisatomi M, Asaumi J, Konouchi H, et al. Assessment of dynamic MRI of Warthin's tumors arising as multiple lesions in the parotid glands. Oral Oncol 2002; 38:369–372.

28. Som PM, Biller HF. High-grade malignancies of the parotid gland: identification with MR imaging. Radiology 1989; 173:823–826.

29. Sigal R, Monnet O, de Baere T. Adenoid cystic carcinoma of the head and neck: evaluation with MR imaging and clinical-pathologic correlation in 27 patients. Radiology 1992; 184:95–101.

30. Freling NJ, Molenaar WM, Vermey A. Malignant parotid tumors: clinical use of MR imaging and histologic correlation. Radiology 1992; 185: 691–696.

31. Swartz JD, Rothman MI, Marlowe FI. MR imaging of parotid mass lesions: attempts at histopathologic differentiation. J Comput Assist Tomogr 1989; 13:789–796.

32. Wang J, Takashima S, Takayama F, et al. Head and neck lesions: characterization with diffusion-weighted echo-planar MR imaging. Radiology 2001; 220:621–630.

33. Sakamoto M, Sasano T, Higano S, et al. Usefulness of heavily T2 weighted magnetic resonance images for the differential diagnosis of parotid tumors. Dentomaxill Radiol 2003; 32:295–299.